energies

MDPI

Article

Novel Intelligent Control Technology for Enhanced Stability Performance of an Ocean Wave Energy Conversion System

Kai-Hung Lu [1,2], Chih-Ming Hong [3,*], Xiaojing Tan [1,2] and Fu-Sheng Cheng [4]

[1] School of Electronic and Electrical Engineering, Minnan University of Science and Technology, Quanzhou 362700, China; khluphd@gmail.com (K.-H.L.); no07210815@yahoo.com (X.T.)
[2] Fujian Key Laboratory of Industrial Automation Control Technology and Information Processing, Quanzhou 362700, China
[3] Department of Electronic Communication Engineering, National Kaohsiung University of Science and Technology, Kaohsiung 811213, Taiwan
[4] Department of Electrical Engineering, Cheng-Shiu University, Kaohsiung 83347, Taiwan; k0044@gcloud.csu.edu.tw
* Correspondence: d943010014@gmail.com

Abstract: In this article, a novelty control structure of grid-connected doubly-fed induction generator (DFIG) based on a function link (FL)-based Wilcoxon radial basis function network (FLWRBFN) controller is proposed. The back-propagation (BP) method is used online to train the node connecting weights of the FLWRBFN. To improve the online learning capability of FLWBFN, differential evolution with particle swarm optimization (DEPSO) is used to tune the learning rates of FLWRBFN. For high randomness of wave energy generation, the transmission power between generators and electrical grids is easy to unstable and AC bus voltage and DC voltage will also lose constant under the conditions of variable generator speed and variable load. Therefore, the proposed intelligent controller can maintain the above power balance and voltage constant and reduce fluctuation. Finally, PSCAD/EMTDC software is used to simulate and study various cases to confirm the robustness and usefulness of the proposed intelligent control technology applied to an ocean wave energy conversion system.

Keywords: function link-based Wilcoxon radial basis function network controller (FLWRBFN); wave energy conversion system (WECS); differential evolution with particle swarm optimization (DEPSO); doubly-fed induction generator (DFIG)

Citation: Lu, K.-H.; Hong, C.-M.; Tan, X.; Cheng, F.-S. Novel Intelligent Control Technology for Enhanced Stability Performance of an Ocean Wave Energy Conversion System. *Energies* **2021**, *14*, 2027. https://doi.org/10.3390/en14072027

Academic Editor: Matthew Lewis

Received: 26 February 2021
Accepted: 2 April 2021
Published: 6 April 2021

1. Introduction

As the world's energy demand continues to grow and conventional fossil energy such as oil, natural gas and coal are increasingly exhausted. Therefore, clean energy such as solar, wind, tidal and biomass, etc., is becoming a necessity. Wave energy is one of the most plentiful and common marine energy resources. The wave motion of seawater can produce huge amounts of energy, thus captivating the attention of many countries, many of which are working to actively develop it [1–3].

The vast marine resources provide a shallow and rich environment for the exploitation of modern energy. In order to simplify the hypothesis, literature [4,5] defined the energy extraction and control of the optimized ocean wave energy converter. Although wave energy engineering has begun to develop, the energy conversion characteristics and related researches of large WEC are rather limited. A well-designed turbine with a properly controlled electric drive can work at low airspeed, but the average power generated is low. Such performance is unfavorable for energy generation [6]. Hence, the power characteristics of the wave energy conversion system (WECS) are limited, and its economy is far inferior to other renewable energy sources. Therefore, it is urgent to improve and stabilize the capacity element of the intelligent control system [7,8]. In addition, three-phase DFIG is

diffusely adopted in renewable power conversions, such as wind energy generation and small hydropower plants, and is used independently and transmitted to the electrical grid.

The most common use of WECS or wind turbine in power systems is the crowbar protection strategy. Because the fluctuation of the grid voltage will cause the large current of the wind turbine, to make the generator stabilize the transient process of excessive, the resistance short-connected rotor winding is usually designed to bypass the rotor side converter, which releases the large current of the rotor side and the excess energy of the unit, so as to protect the grid-connected converter [9–11]. The commonly used passive crowbar protection circuit technology cannot transmit active or reactive power to the electrical grid during grid failure or fluctuation; thus, it cannot help the power grid to recover. Accordingly, it cannot meet the requirements of low voltage through the production of wind turbines connected to the electrical grid. Therefore, a novel and efficient control strategy for grid and rotor side converter is proposed to improve the low voltage ride through (LVRT) capability of the DFIG wind turbine in [12].

Particle Swarm Optimization (PSO) and Differential Evolutionary (DE) algorithms are random parallel optimization methods based on the swarm optimization algorithm. They optimize a search by heuristic swarm intelligence and are successfully applied to many engineering problems [13,14]. Many studies have also developed some improved PSO and DE algorithms to increase the search behavior and accuracy of original PSO and DE. Among all kinds of optimization algorithms, DE is an efficient, parallel and heuristic global optimization algorithm and is famous for its few parameters. In addition, PSO is a kind of random optimization technology designed to simulate the behavior of birds, which relies on information sharing and exchange between individuals and populations and can validly resolve complex optimization problems. According to the advantages of each algorithm, the combination of these algorithms can improve the search performance [15]. A mixed algorithm of DE and PSO is developed in this paper. The slow convergence in DE can be resolved by PSO while easily trapping to the local optimum of PSO improved by DE. Moreover, DEPSO has a high accuracy of output for searching performance and reduces computational time [16,17].

Although in recent years, some intelligent control schemes based on fuzzy logic with sliding mode controller, direct power and torque control (DPTC), perturb and observe (P&O) and Grey-based Elman neural network have been proposed for the external controllers of wind energy conversion. These intelligent controllers can improve control performance, but there is still room for improvement [18–20]. The Wilcoxon neural network studied in this paper is robust to the uncertainties, randomness, and parameter changes of the WECS, and can effectively restrain the external disturbance to the system. It is widely used in control systems to achieve better dynamic performance. In addition, in order to further enhance the control ability of Wilcoxon radial basis function network (WRBFN), the function-link neural network (FLNN) is used. FLNN uses the stochastic linear combination to input signals, expands the input signal space, successfully omits the hidden layer in multi-layer perceptron, simplifies the architecture of multi-layer perceptron, and makes the structure of FLNN have faster convergence speed and less computational amount than that of multi-layer perceptron. In addition, FLNN can be extended to the higher-order part because of the input variables, which can more effectively approximate the non-linear function [21–24]. Therefore, for the application of instant control system, FLNN is quite suitable. Thus, the function link-based Wilcoxon radial basis function network (FLWRBFN) controller is proposed, which can change the network structure to achieve faster convergence.

In this paper, the simulation models of WECS variable speed operation and intelligent control strategy are established under the software environment of PSCAD/EMTDC and MATLAB, respectively. The main contributions are (1) a DEPSO-based FLWRBFN is proposed and applied to the grid-connected DFIG-Wells turbine system, and (2) a Lyapunov analysis of stability for the control scheme against WECS uncertainties and disturbances. The performance results show that the proposed control scheme can effectively damping

power oscillation in power system changes and short-circuit faults, and ensure the dynamic and transient performance of WECS in a wide range of different conditions.

2. Modeling of the Studied System

The variable speed Wells turbine driving a DFIG system can be described as follows:

2.1. Structure of the System

Figure 1 is the schematic of a DFIG-based Wells turbine system. The DFIG is driven by the Wells turbine is to obtain maximum power and send it to the grid. An AC-DC converter is designed, which converts the AC power generated by the DFIG into DC power. The proposed direct-drive DFIG system used both rotor-side and stator-side converter, and a Z-source converter between the rotor slip rings. Therefore, an effective method based on FLWRBFN with DEPSO control system is proposed for wave period variations of the turbine or load changes and controls the electromagnetic torque of a DFIG driven using the variable speed Wells turbine, and the effects of different speed variation forms are considered.

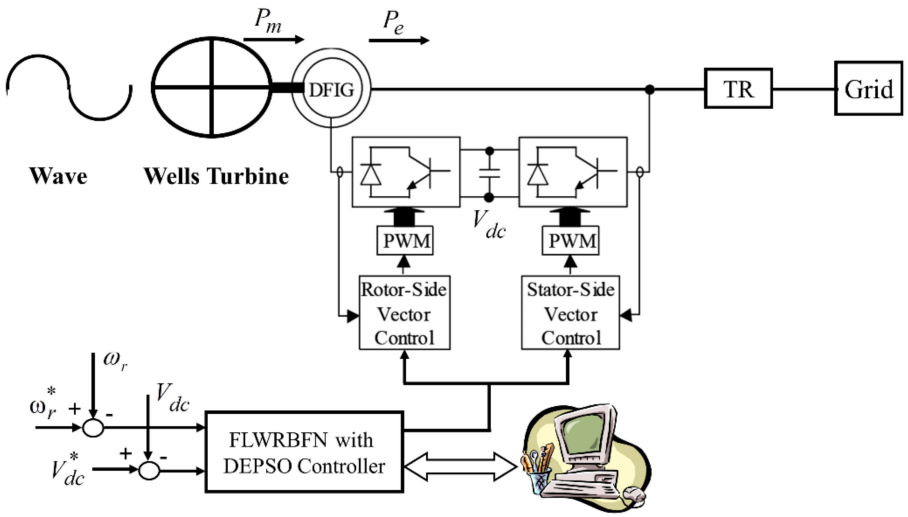

Figure 1. Schematic of a DFIG-based Wells turbine system.

2.2. Wave Energy Characteristics

DFIG of Wells turbines includes a set of asynchronous wound generators, a PWM converter system and a control system. Its stator winding is directly connected with the power grid, and the electric energy from the generator is directly input into the power grid through the stator winding. From Figure 1, the wound rotor is connected to a set of back-to-back power converters, one of which is close to the rotor side and the other is close to the grid side; both are bidirectional converter architectures. The two are connected by a DC capacitor link. The detailed mathematical model of DFIG system converting a-b-c three-axis component into a d-q two-axis component, control models, and the torque equations can be used for reference [21,22], respectively.

The airflow generated by oscillating water column (OWC) wave energy is reciprocating. It is necessary to install a Wells turbine, which can rotate in the same direction in the airflow passage under the action of two-way airflow. The incoming and outgoing airflow will drive the Wells turbine to rotate and then drive generators to generate power, thus greatly improving the airflow rate and thus increasing the efficiency of the system. According to linear wave theory, based on monochromatic waves of deep water, the wave power P_{wave} is as follows [25]

$$P_{wave} = \frac{\rho g^2 H^2 T}{32\pi} \quad [\mathrm{W/m}] \tag{1}$$

where ρ, g and H refer to the ocean water density, gravitational acceleration and wave height, respectively. T is the wave period.

2.3. Wells Turbine Modeling

The produced torque (T_m) obtained from wave energy, torque coefficient (C_t), and the angle of incidence of air on the turbine blade (α) of the studied Wells turbine can be calculated by combining Equations (2)–(4), respectively [26,27].

$$T_m = kC_t\left(\mathrm{V_A^2} + \mathrm{V_B^2}\right) \tag{2}$$

$$C_t = C_8 + \frac{C_1\alpha^3 - C_{23}\alpha^2 + C_3\alpha - C_4}{C_5\alpha^2 + C_6\alpha - C_7} \tag{3}$$

$$\alpha = \tan^{-1}\left(\frac{\mathrm{V_A}}{\mathrm{V_B}}\right) \tag{4}$$

where $\mathrm{V_A}$ and $\mathrm{V_B}$ represent the axial velocity and blade tip velocity (m/s), respectively, k is the coefficient of the Wells turbine and C_1 to C_8 are the power coefficients.

2.4. DFIG Modeling

In a three-phase system, the voltage and torque equations of DFIG are both nonlinear and time-varying, so its torque control is more complex. Therefore, the three-phase instantaneous value of the original balance can be converted to the d-q reference frame and rotates by using the synchronous rotating coordinate method [12]. The peak value and phase angle of the three-phase sinusoidal wave can be controlled by controlling the q-axis and the d-axis. Therefore, according to the system voltage, produced torque (T_m) and electromagnetic torque (T_e) equations in [11,28], the following are obtained:

$$T_m = \frac{P_m}{\omega_r} \tag{5}$$

$$T_e = \frac{P_e}{\omega_e} = \frac{P_e}{\omega_r} \tag{6}$$

The mechanical dynamic equation of the DFIG is shown in the following equation

$$J\frac{d\omega_r}{dt} = T_m - B\omega_r - T_e \tag{7}$$

where ω_r is the rotor angular frequency, ω_e is the electrical angular frequency, J is the total inertia moment at the rotor of the DFIG, and B is the coefficient of friction.

3. Design of the Novel FLWRBFN with DEPSO Control System

The linear Wilcoxon regressor method is very sensitive to outliers and has strong robustness, so the Wilcoxon neural network is further developed [29,30]. The proposed FLWRBFN in this paper is shown in Figure 2 as a four-layer network structure. The FLWRBFN control system is expanded by using FLNN to increase the accuracy of function approximation. The FLWRBFN with DEPSO controller is used to generate control signal i_d^* from FLWRBFN. FLNN extends input signals to functions that are linearly independent of each other by function expansion. In this article, the trigonometric function is used for function expansion, which is simple and easy to calculate. In addition, considering the outer product term of input variables can enhance the approximation ability of functions, and it also provides better performance.

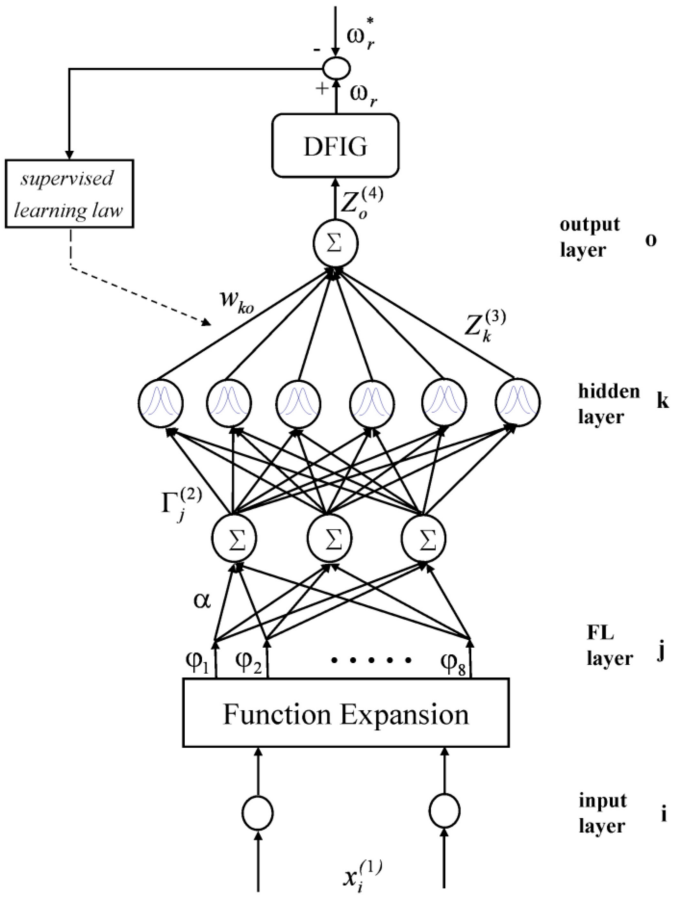

Figure 2. The structure of a FLWRBFN.

3.1. Function-Link Based Wilcoxon Radial Basis Function Network (FLWRBFN)

The input of FLWRBFN is $x_1^{(1)}$ and $x_2^{(1)}$ in the first layer, and $x_1^{(1)}$ is the error between the reference rotor speed ω_r^* and the rotor speed feedback ω_r. $x_2^{(1)}$ is the error between reference DC voltage V_{dc}^* and actual DC voltage V_{dc}. In the proposed FLWRBFN in this paper, the input layer of two neurons, the functional link layer of eight outputs, the hidden layer of 24 neurons and the output layer of 1 neuron.

First Layer: Input Layer

The main purpose of neurons in this layer is to directly transmit signals. Thus, for the *i*th node of first layer, its input and output are as follows:

$$net_i^{(1)} = x_i^{(1)}(N) \tag{8}$$

$$Z_i^{(1)}(N) = net_i^{(1)}(N)\ i = 1, 2 \tag{9}$$

where $x_i^{(1)}$ is the input values, $net_i^{(1)}$ and $Z_i^{(1)}$ are the input and output of the *i*th node in layer 1, respectively. *N* represents the *N*th iteration

Second Layer: FL Layer

The second layer is the function expansion layer, which mainly expands the input signals of the first layer into linear independent functions. Therefore, in this layer, the input variables $[x_1\ x_2]$ are extended to $\phi_E = [\phi_1, \phi_2 \cdots, \phi_8] = [1, x_1, \sin(\pi x_1), \cos(\pi x_1), x_2, \sin(\pi x_2), \cos(\pi x_2), x_1 x_2]$. The second layer output $\Gamma_j^{(2)}$ of the extended input variable is:

$$\Gamma_j^{(2)}(N) = \sum_{E=1}^{8} \phi_E(x_i) \cdot \alpha_{Ej}\ j\ = 1 \sim 3 \tag{10}$$

where $\alpha_{Ej} = \begin{bmatrix} \alpha_{11} & \alpha_{12} & \alpha_{13} & \cdots & \alpha_{81} & \alpha_{82} & \alpha_{83} \end{bmatrix} \in R^{1\times 24}$ is the connective weight vector.

Third Layer: Hidden Layer

Each neuron represents the characteristics of a membership function in this layer. Here, the Gaussian function is used as the membership function of the neurons in this layer, because the Gaussian function is a particular example of a radial basic function. Thus, this layer input and output are obtained as follows:

$$net_k^{(3)}(N) = -\sum_{j=1}^{n} \left(\Gamma_j^{(2)} - c_{jk}\right)^2 / v_{jk} \tag{11}$$

$$Z_k^{(3)}(N) = \exp\left(net_k^{(3)}(N)\right) \; k = 1, \ldots, 6 \tag{12}$$

where $net_k^{(3)}$ and $Z_k^{(3)}$ are the input and output of the kth node in layer 3. $c_{jk} = [c_{1k} c_{2k} \cdots c_{jk}]^T$ denote the center value of the Gaussian function. v_{jk} is the width of the Gaussian function.

Fourth Layer: Output Layer

This layer is the last layer of FLWRBFN and also the output layer. The operation of this layer is to add all the output of the hidden layer.

$$net_o^{(4)} = \sum_{k=1}^{m} w_{ko} Z_k^{(3)}(N) \; k = 1, \ldots, 6 \tag{13}$$

$$Z_o^{(4)}(N) = net_o^{(4)}(N) \; k = 1, \ldots, 6 \tag{14}$$

where the connection weight w_{ko} is the connective weight between the hidden and the output layer o. $Z_o^{(4)}$ is the control effort of the control system, i.e., $Z_o^{(4)} \equiv i_{dr}^*$ is rotor side converter; moreover, $Z_o^{(4)} \equiv i_{ds}^*$ is stator side converter.

3.2. Learning and Training Procedures of FLWRBFN

In this study, FLWRBFN can train the weight of neurons to enhance the dynamic property of the network. In this way, the dynamic response of the neural network can be better than that of the general NN through the process of changing the weights. Thus, to describe the gradient vector obtained during the online training of FLWRBFN, the output direction of each neuron is calculated in the opposite direction. Then, a cost function E is defined as:

$$E = \frac{1}{2}(\omega_r^* - \omega_r)^2 = \frac{1}{2} e_c^2 \; k = 1, \ldots, 6 \tag{15}$$

Then, the learning rules and update of FLWRBFN weights are described as follows. Firstly, the weight w_{ko} is updated from the fourth layer. The error item returned from this layer and updated term are given by Equations (16) and (17).

$$\delta_o = -\frac{\partial E}{\partial net_o^{(4)}} = \left[-\frac{\partial E}{\partial Z_o^{(4)}} \frac{\partial Z_o^{(4)}}{\partial net_o^{(4)}} \right] \tag{16}$$

$$w_{ko}(N+1) = w_{ko}(N) + L_w \Delta w_{ko}(N) \tag{17}$$

Here, $\Delta w_{ko} = \frac{\partial E}{\partial w_{ko}} = \delta_o Z_k^{(3)}$ is the adjusted value of w_{ko}. L_w is the learning rate for w_{ko}. Then, the weights c_{jk} and v_{jk} in the third layer are updated by Equations (18) and (19).

$$c_{jk}(k+1) = c_{jk}(k) + L_m \Delta c_{jk} \tag{18}$$

$$v_{jk}(k+1) = v_{jk}(k) + L_\sigma \Delta v_{jk} \tag{19}$$

where L_m is the learning rates of c_{jk}. L_σ is the learning rates of v_{jk}.

The adaptive rules for c_{jk} and v_{jk} are shown in the following Equations (20) and (21).

$$\Delta c_{jk} = -\frac{\partial E}{\partial c_{jk}} = \left[-\frac{\partial E}{\partial net_o^{(4)}} \frac{\partial net_o^{(4)}}{\partial Z_k^{(3)}} \frac{\partial Z_k^{(3)}}{\partial c_{jk}} \right] = \delta_o w_{ko} Z_k^{(3)} \frac{2\left(\Gamma_j^{(2)} - c_{jk}\right)}{v_{jk}} \tag{20}$$

$$\Delta v_{jk} = -\frac{\partial E}{\partial v_{jk}} = \left[-\frac{\partial E}{\partial net_o^{(4)}} \frac{\partial net_o^{(4)}}{\partial Z_k^{(3)}} \frac{\partial Z_k^{(3)}}{\partial v_{jk}} \right] = \delta_o w_{ko} \frac{2\left(\Gamma_j^{(2)} - c_{jk}\right)^2}{\left(v_{jk}\right)^2} \tag{21}$$

In the process of searching for solutions, if the learning rate is too large, the search will not be carefully done and the optimization solutions may be missing, the system may become unstable. The learning rate is too low; although the weight learning will be more careful, it will make the search process too slow [20,31]. The value of the learning rate is between 0 and 1. The common choice of learning rate is a trial-and-error method. Therefore, it is very important to set the learning rates. Therefore, this paper proposes DEPSO to adjust learning rates (L_w,L_m,L_σ) of FLWRBFN online, which is introduced in the following section.

3.3. DEPSO Online Adjusts Learning Rate

The DEPSO part of this algorithm combines DE into PSO by separating the logic algorithm in the different round of work by odd and even round, but it shares the particle for a better solution because of the time the PSO value becomes the local value [32–35]. It is probably not the best value, so DE helps this problem and most of the time, DE computes this over a long period of time. PSO was the best algorithm with the best speed computation, it can help DE with that problem. Thus, DEPSO may not allow the PSO to have a long period of computation and the result may not be stuck at the local minimum. In order to further enhance the ability of FLWRBFN itself to process dynamic information through online learning of its own neural network, this paper proposes the DEPSO algorithm to tune the learning rates of L_w, L_m and L_σ of FLWRBFN. The DEPSO combines the characteristics of DE and PSO. The process is obtained as follows:

Step 1: Initial population.

Step 2: The DE and PSO algorithms are calculated separately, and the initial population is assessed. That is, the fitness of each individual in the initial population is calculated, and a better algorithm is selected to evolve. For each agent, a fitness value is evaluated. A suitable fitness function, FIT, is selected for the following equation in order to calculate the fitness value:

$$FIT = \frac{1}{0.1 + abs(\omega_r - \omega_r^*) + abs(V_{dc} - V_{dc}^*)} \tag{22}$$

where the adds 0.1 to the denominator to keep *FIT* from approaching infinity.

Step 3: In the odd generation, the selected algorithm of step 2 shares the better result to another by iteration to enhance the performance and convergence by the better result.

Step 4: In even generations, DE and PSO will calculate each other's fitness values and compare their advantages and disadvantages, and choose better algorithms to enter the next generation.

Step 5: Suppose that the termination condition is not met, return to step 2.

Step 6: Repeat steps 2–5 until the optimal fitness is significantly increased or the set count of a generation is reached. Finally, the highest-level fitness value is chosen as the best learning rates (L_w,L_m,L_σ) of the FLWRBFN.

4. Analysis of Convergence

Choice of the value of the learning rate coefficients of the FLWRBFN has a major effect on the network property. Thus, so as to train the FLWRBFN effectually, the varied learning rates, which assure the convergence of the output tracking errors based on the analysis of a discrete-type Lyapunov function [36,37]. The objective of the convergence analysis is

to derive particular learning rates for network parameters to ensure the convergence of the control. Considering the cost function E shown in (15) as a discrete-type Lyapunov function, the change in the Lyapunov function can be received by:

$$\Delta E(N) = E(N+1) - E(N) \tag{23}$$

Then, the linearized model [33] of the error equation can be expressed by (20) and (21):

$$\begin{aligned} &E(N+1) = E(N) + \Delta E(N) \\ &= E(N) + \sum_{k=1}^{6}\left[\frac{\partial E(N)}{\partial w_{ko}}\Delta w_{ko}\right] + \sum_{j=1}^{3}\sum_{k=1}^{6}\left[\frac{\partial E(N)}{\partial c_{jk}}\Delta c_{jk} + \frac{\partial E(N)}{\partial v_{jk}}\Delta v_{jk}\right] \\ &= \tfrac{1}{3}E(N) - L_w\sum_{k=1}^{6}\left[\frac{\partial E(N)}{\partial Z_o^{(4)}}\frac{\partial Z_o^{(4)}}{\partial w_{ko}}\right] + \tfrac{1}{3}E(N) - L_m\sum_{j=1}^{3}\sum_{k=1}^{6}\left[\frac{\partial E(N)}{\partial Z_o^{(4)}}\frac{\partial Z_o^{(4)}}{\partial Z_k^{(3)}}\frac{\partial Z_k^{(3)}}{\partial c_{jk}}\right] \\ &+\tfrac{1}{3}E(N) - L_\sigma\sum_{j=1}^{3}\sum_{k=1}^{6}\left[\frac{\partial E(N)}{\partial Z_o^{(4)}}\frac{\partial Z_o^{(4)}}{\partial Z_k^{(3)}}\frac{\partial Z_k^{(3)}}{\partial v_{jk}}\right] \end{aligned} \tag{24}$$

where w_{ko}, c_{jk} and v_{jk} represent the change in the weight in the fourth layer, the center value of the Gaussian function and the width of the Gaussian function in the third layer, respectively. If the learning rate coefficients of the FLWRBFN are devised as:

$$L_w = \frac{E(N)}{3\left[\sum_{k=1}^{6}\left(\frac{\partial E(N)}{\partial Z_o^{(4)}}\frac{\partial Z_o^{(4)}}{\partial w_{ko}}\right)^2 + \varepsilon\right]} \tag{25}$$

$$L_m = \frac{E(N)}{3\left[\sum_{j=1}^{3}\sum_{k=1}^{6}\left(\frac{\partial E(N)}{\partial Z_o^{(4)}}\frac{\partial Z_o^{(4)}}{\partial Z_k^{(3)}}\frac{\partial Z_o^{(3)}}{\partial c_{jk}}\right)^2 + \varepsilon\right]} \tag{26}$$

$$L_\sigma = \frac{E(N)}{3\left[\sum_{j=1}^{3}\sum_{k=1}^{6}\left(\frac{\partial E(N)}{\partial Z_o^{(4)}}\frac{\partial Z_o^{(4)}}{\partial Z_k^{(3)}}\frac{\partial Z_o^{(3)}}{\partial v_{jk}}\right)^2 + \varepsilon\right]} \tag{27}$$

where ε is a positive constant. Hence, (23) can be revised as:

$$\begin{aligned} E(N+1) &\approx \varepsilon(L_w + L_m + L_\sigma) \\ &= \frac{E(N)\varepsilon}{3\left[\sum_{k=1}^{6}\left(\frac{\partial E(N)}{\partial Z_o^{(4)}}\frac{\partial Z_o^{(4)}}{\partial w_{ko}}\right)^2 + \varepsilon\right]} \\ &= \frac{E(N)\varepsilon}{3\left[\sum_{j=1}^{3}\sum_{k=1}^{6}\left(\frac{\partial E(N)}{\partial Z_o^{(4)}}\frac{\partial Z_o^{(4)}}{\partial Z_k^{(3)}}\frac{\partial Z_o^{(3)}}{\partial c_{jk}}\right)^2 + \varepsilon\right]} \\ &= \frac{E(N)\varepsilon}{3\left[\sum_{j=1}^{3}\sum_{k=1}^{6}\left(\frac{\partial E(N)}{\partial Z_o^{(4)}}\frac{\partial Z_o^{(4)}}{\partial Z_k^{(3)}}\frac{\partial Z_o^{(3)}}{\partial v_{jk}}\right)^2 + \varepsilon\right]} \\ &< \frac{E(N)}{3} + \frac{E(N)}{3} + \frac{E(N)}{3} = E(N) \end{aligned} \tag{28}$$

In accordance with (15) and (28), the convergence of the cost function E can be guaranteed. Thus, the tracking error of the WECS will bring the convergence to zero as $t \to 0$ if the learning rates of the FLWRBFN are devised as (25) to (27).

5. Simulation Results and Case Studies

The simulation is divided into two case studies to simulate the dynamic and transient performance of wave power generation system under different disturbances and faults. To test the robustness of the proposed FLWRBFN with DEPSO, proportional-integration (PI), RBFN and FLWRBFN techniques are compared through various tests. The performance of each scheme in WECS control are shown in Figures 3–6, and the quantize values are clearly summarized in Tables 1–4. Two cases show the effectiveness and robustness of the FLWRBFN with DEPSO. Various parameters of WECS used in this paper are as follows: S_{DFIG} = 20 MW, 3.76 A, 3000 r/min, T_R = 0.69/33 kV, J = 0.00132 Nm s2, B = 0.00577 Nm s/rad, V = 15 KV, PF = 0.976, f = 60 Hz, C_{dc} = 0.6 pu.

The simulation cases are to analyze the effect of DFIG for rotor speed response, power change, and bus voltage transient process when serious load disturbance and short circuit faults suddenly occur in the electrical grid. The proposed intelligent control scheme has a better identification effect for nonlinear dynamic systems and can be applied to DFIG-based WECS to improve the overall dynamic performance.

5.1. Load Change

In this simulation case, the load rises rapidly from 0.5 pu to 1 pu at 4 s and then decreases from 1 pu to 0.5 pu at 10 s. From Figure 3a, it can be observed that the rotor speed of the DFIG with PI controller has the longest oscillation time and the largest oscillation amplitude, followed by RBFN controller. With the WECS of FLWRBFN with DEPSO, the rotor speed of DFIG can quickly return to a stable state in a few cycles around 1 s. It could be clearly seen from Figure 3b,c that when FLWRBFN with DEPSO controller is implemented compared with the other two controllers, the proposed control scheme can minimize the oscillation, overshoot and instability of AC and DC link voltages of DFIG when disturbances occur, and the time to return to stability is also the fastest. From Figure 3b,c, it is also found that when FLWRBFN is used, the time of the AC line and DC link voltage return to stability is the fastest, and the bus voltage is maintained at 1 pu. The dynamic response of the real power on the grid side is shown in Figure 3d. Similarly, the results from Figure 4d show that when the load changes in 4 s and 10 s, the real power response of FLWRBFN with DEPSO control has small amplitude change and the fastest convergence time. Although all three technologies can return to the steady state, the PI control has the largest variety in the amplitude of the real power response and the slowest convergence time, followed by RBFN, while the proposed FLWRBFN with DEPSO has the smallest fluctuations and faster real power recovery, returning to the stable state within about 0.9 s. Therefore, from the results of Figure 3, we can see that the proposed FLWRBFN with DEPSO has a faster tracking speed, more stable output power and better control effect for the variation of real power and voltage. In addition, to verify the convergence ability of FLWRBFN with DEPSO, it compares three other intelligent algorithms (MPSO [38], PSO and without PSO), as shown in Figure 4, and quantifies each performance index in Table 1. Table 1 shows that the FLWRBFN with DEPSO for WECS has the best accuracy and faster convergence speed compared with other methods. These results prove that FLWRBFN with DEPSO can obtain better control of nonlinear dynamic systems than other methods.

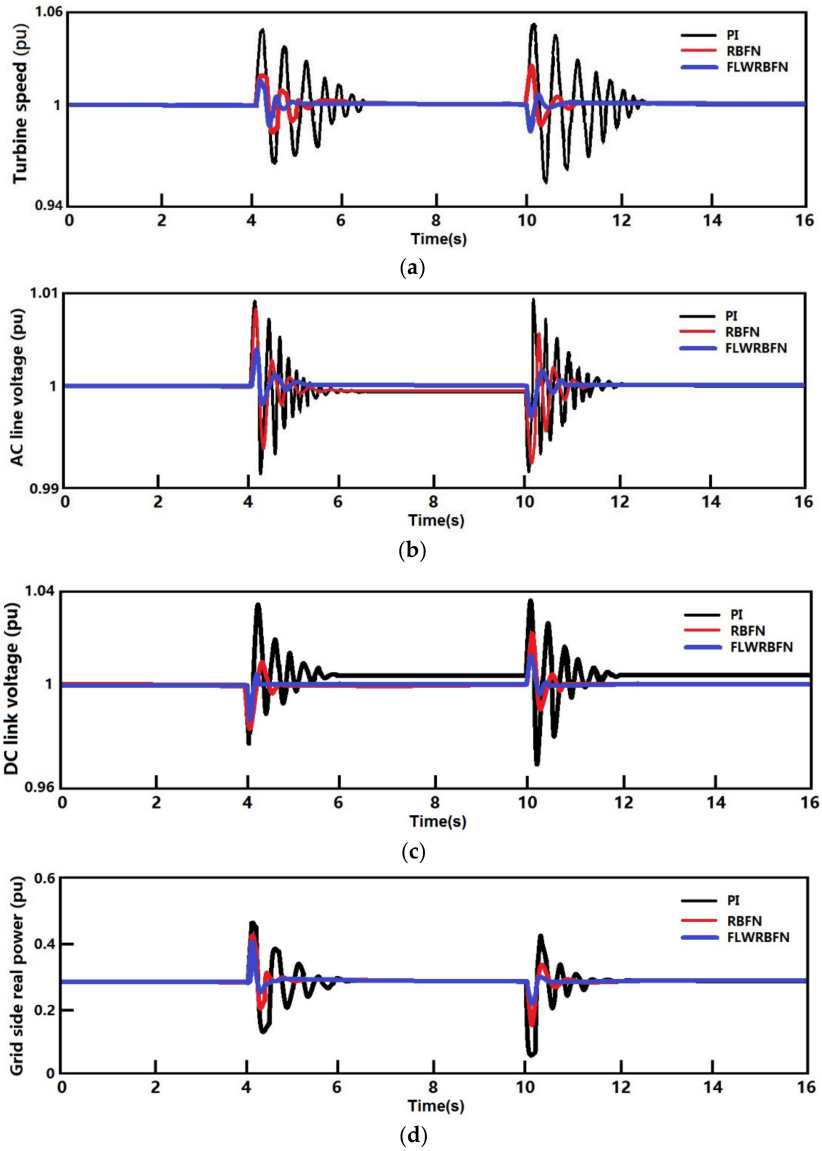

Figure 3. The dynamic simulation results of the studied system under load change: (**a**) Turbine speed; (**b**) AC line voltage; (**c**) DC link voltage; (**d**) Grid side real power.

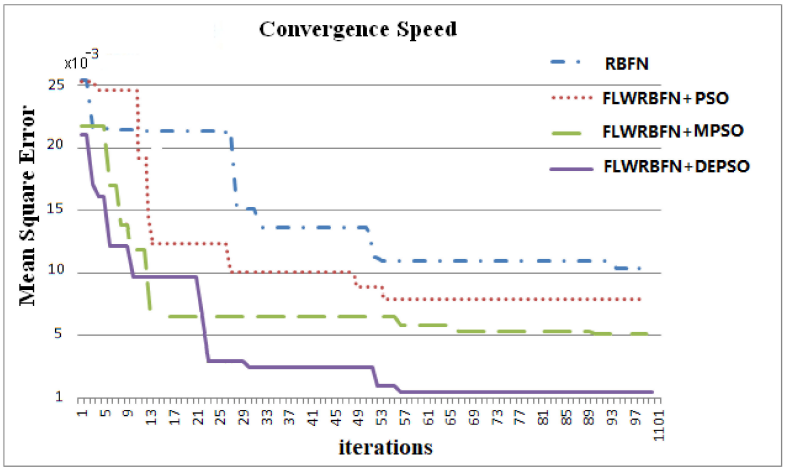

Figure 4. Convergence speed of the different methods under load disturbance.

Table 1. Quantitative comparison for several methods with load change.

Method	Iterative Number	CPU Run Time (10^2 s)	Mean Square Error (10^{-3})	Accuracy (%)
FLWRBFN + DEPSO	57	1.48	1.235	98.76
FLWRBFN + MPSO	90	2.34	5.017	94.98
FLWRBFN + PSO	54	1.40	7.581	92.42
RBFN	94	2.44	10.051	89.95

5.2. Short Circuit Fault

This case is to simulate the transient response state of WECS when a short circuit fault seriously affects the safety and stability of the studied system. In this simulation, the three-phase short-circuit fault is set beside the generator bus. The transient characteristics of each parameter of the WECS, as shown in Figure 5.

Figure 5a presents the rotor speed response of DFIG. From the result, the rotor speed using FLWRBFN with DEPSO for DFIG returns to a stable state at about 5 s, and the oscillation is also the minimum after fault clearing. Figure 5b illustrates the AC bus voltage dynamic response when a short circuit fault occurs. From Figure 5b, it can be clearly noticed that when the short circuit is added, the voltage of the AC bus drops to 0.3 pu. After fault clearing, it can be seen that the proposed method can make the voltage return to the stable value as soon as possible. However, in terms of the voltage response of the three methods, the PI method can recover slowly to steady state at about 2.5 s, and the voltage overshoot and undershoot are also the largest. The same is true for the transient response of DC voltage. Among the three methods, PI method makes DC voltage the most unstable, the FLWRBFN with DEPSO method has the best robustness, with RBFN having the second-best. The transient response of the real power on the grid side is shown in Figure 5d. The PI method has the largest real power fluctuations, and it will return to stability in about 6.1 s, while the FLWRBFN with DEPSO method has the smallest real power fluctuation—it only needs a few cycles to return to the stable value.

In order to confirm the convergence ability of FLWRBFN with DEPSO, the performance comparisons with the four other algorithms are given in Figure 6, and quantifies each performance index in Table 2. Table 2 illustrates that the FLWRBFN with DEPSO for WECS has the best accuracy and fastest convergence speed compared with other methods. These results prove that FLWRBFN with DEPSO can obtain better control of nonlinear dynamic systems than other methods. These results show the convergence property and transient stability of various schemes, and also represent that when FLWRBFN with DEPSO is put into use in WECS, it can effectively reduce the oscillation of rotor speed, AC bus, DC link voltage and real power caused by fault occurrence, and can quickly return to the steady state, so as to achieve a better control effect.

To verify the real time online adjustment of FLWRBFN learning rates by DEPSO, WECS can obtain the best transient and dynamic response under the condition of a load change and short circuit. Therefore, Tables 3 and 4 compare the proposed technique with other three intelligent algorithms, RBFN, FLWRBFN+PSO, and FLWRBFN+MPSO, in terms of system behaviour on the grid side. From the results, it can be observed that the provided FLWRBFN+DEPSO has a better effect on voltage regulation and voltage oscillation in terms of load changes and short-circuit faults.

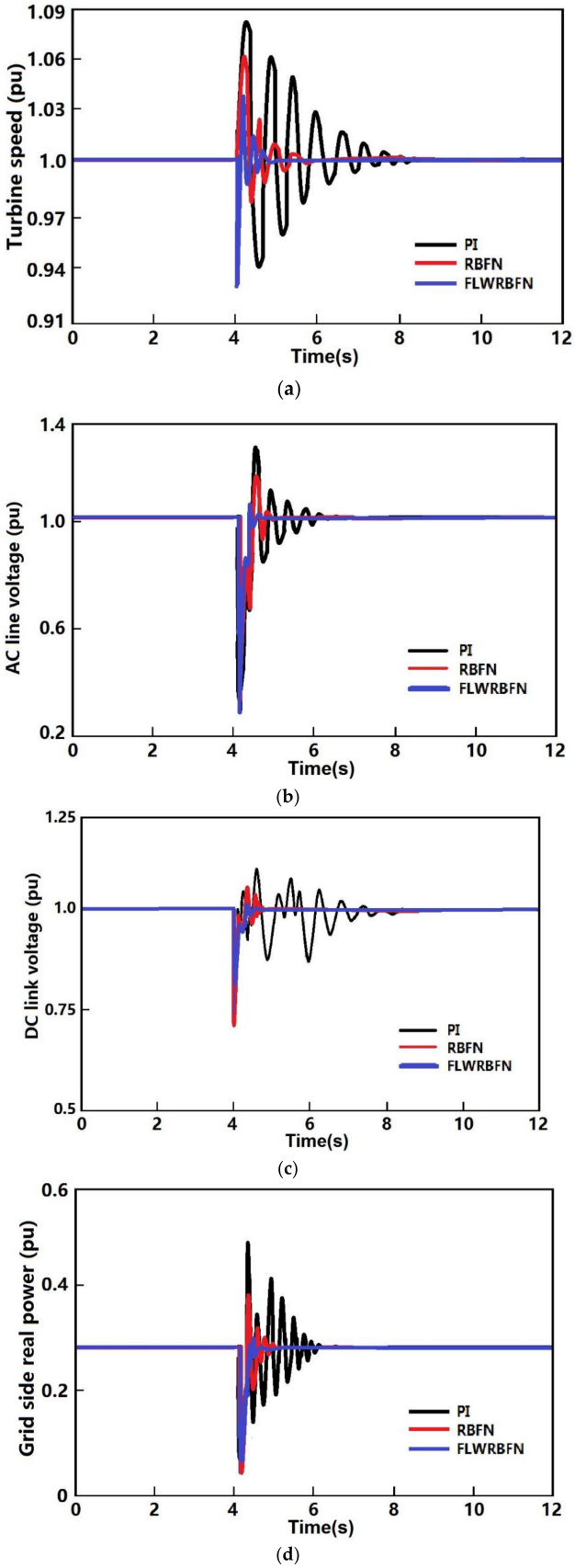

Figure 5. The transient simulation results of the studied system under short circuit: (**a**) Turbine speed; (**b**) AC line voltage; (**c**) DC link voltage; (**d**) Grid side real power.

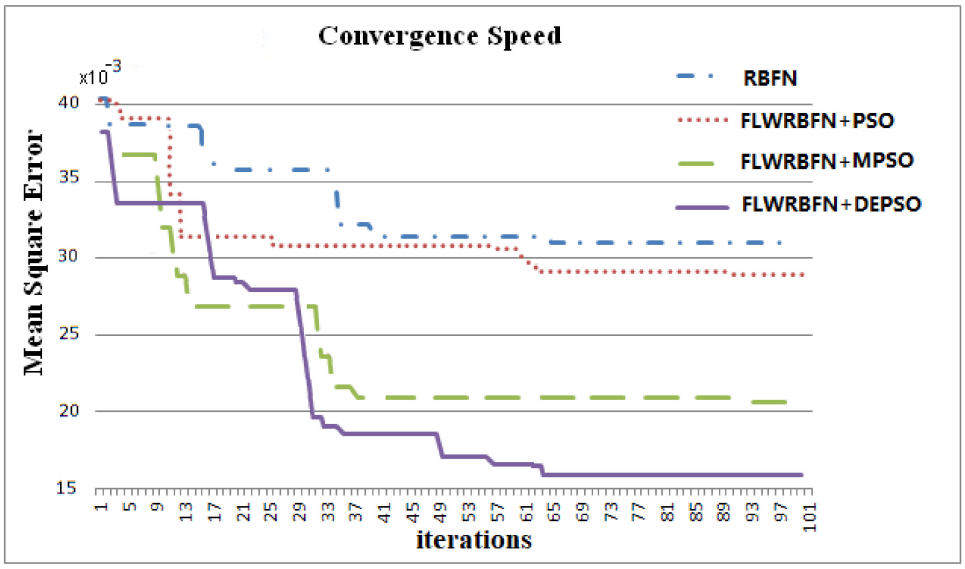

Figure 6. Convergence speed of the different algorithms under short circuit.

Table 2. Quantitative comparison for several methods with short-circuits.

Methods	Interative Number	CPU Run Time (10^2 s)	Mean Square Error (10^{-3})	Accuracy (%)
FLWRBFN + DEPSO	64	1.66	15.965	84.03
FLWRBFN + MPSO	94	2.44	20.071	79.93
FLWRBFN + PSO	91	2.36	29.057	70.94

Table 3. System dynamic behavior comparison with load change [18,39].

Method	FLWRBFN + DEPSO	FLWRBFN + MPSO	FLWRBFN + PSO	RBFN
Grid-Side Voltage	1.0003125	1.0005316	1.0004338	0.9976911
DC-Side Voltage	1.0012123	1.0026557	1.0013670	0.9896110
Max. Transient Over Shoot Voltage	1.0043437	1.0060341	1.0071922	1.0085975
Max. Transient Under Shoot Voltage	0.9965313	0.9954371	0.9957687	0.991125

Table 4. System dynamic behavior comparison with short-circuit fault [18,39].

Method	FLWRBFN + DEPSO	FLWRBFN + MPSO	FLWRBFN + PSO	RBFN
Grid-Side Voltage	1.0204878	1.0257873	1.0310922	1.0214457
DC-Side Voltage	1.006251	1.0069122	1.0052166	1.0071458
Max. Transient Over Shoot Voltage	1.0780488	1.0993411	1.1477012	1.1931707
Max. Transient Under Shoot Voltage	0.9609756	0.0922378	0.0912409	0.0902439

6. Conclusions

The simulation results demonstrate that the proposed FLWRBFN with DEPSO method can effectively improve the parameters of the utility grid and power operation and also highly ensure the stability of the power control. From the case studies, the iteration of the load disturbance case is reduced by 29.6%, and the accuracy is improved by 8.9% over the other approaches. The same, the iteration of the load disturbance case is reduced by 39.3%, and the accuracy is improved by 15.6% over the other approaches in the fault case. The proposed method combines DE with PSO and was applied to the proposed FLWRBFN

algorithm based on function expansion. Through the simulation of load disturbance and short circuit fault, the results show that in the performance of WECS, the proposed algorithm can stabilize the operation of a power grid and enhance the stability of an electrical grid when wave energy generation with high randomness is unstable. In this study, the proposed scheme is also compared with earlier methods. The system dynamic behavior results demonstrate that the proposed technique is robust and provides an excellent performance. In the future, the proposed method can be applied to complex power systems with multiple energy sources. The proposed method should have better damping characteristics. Under unstable conditions, power fluctuations within the power system can effectively stabilize the network.

Author Contributions: K.-H.L. performed the simulations, conducted the concept and application of the software. C.-M.H. contributed to the development algorithm and prepared the original draft of the manuscript to be submitted. X.T. verified the simulation results. F.-S.C. assisted the manuscript preparation. All authors have read and agreed to the published version of the manuscript.

Funding: This research received no external funding.

Data Availability Statement: No new data were created or analyzed in this study. Data sharing is not applicable to this article.

Conflicts of Interest: The authors declare no conflict of interest.

References

1. Halamay, D.A.; Simmons, A.; McArthur, S.; Brekken, T.K.A. Reserve requirement impacts of large-scale integration of wind, solar, and ocean wave power generation. *IEEE Trans. Sustain. Energy* **2011**, *2*, 321–328. [CrossRef]
2. Zhao, X.; Yan, Z.; Zhang, X.-P. A wind-wave farm system with self-energy storage and smoothed power output. *IEEE Access* **2016**, *4*, 8634–8642. [CrossRef]
3. Linda, S.; Rachel, S.; Thomas, D. What drives energy consumers: Engaging people in a sustainable energy transition. *IEEE Power Energy Mag.* **2018**, *16*, 20–28.
4. Romain, G.; Josh, D.; John, V.R. Adaptive control of a wave energy converter. *IEEE Trans. on Sustain. Energy* **2018**, *1*, 1.
5. Nicola, D.; Davide, B.; Francesco, G.; Paolo, C.; Giampaolo, B. Review of oscillating water column converters. *IEEE Trans. Indust. Appl.* **2016**, *52*, 1698–1710.
6. Sunil, K.M.; Aradhna, P. Wells turbine modeling and PI control scheme for OWC plant using Xilinx system generator. In Proceedings of the International Conference on Power, Control & Embedded Systems (ICPCES), Allahabad, India, 9–11 March 2017; pp. 1–6.
7. Francesco, F.; Ringwood, J.V. A simple and effective real-time controller for wave energy converters. *IEEE Trans. Sustain. Energy* **2013**, *4*, 21–30.
8. Bacelli, G.; Nevarez, V.; Coe, R.G.; Wilson, D.G. Feedback Resonating Control for a Wave Energy Converter. *IEEE Trans. Ind. Appl.* **2019**, *56*, 1862–1868. [CrossRef]
9. Foster, S.; Xu, L.; Fox, B. Coordinated reactive power control for facilitating fault ride through of doubly fed induction generator- and fixed speed induction generator-based wind farms. *IET Renew. Power Gener.* **2010**, *4*, 128–138. [CrossRef]
10. López, J.; Gubía, E.; Olea, E.; Ruiz, J.; Marroyo, L. Ride through of wind turbines with doubly fed induction generator under sym-metrical voltage dips. *IEEE Trans. Ind. Electron.* **2009**, *56*, 4246–4254. [CrossRef]
11. Meegahapola, L.G.; Littler, T.; Flynn, D. Decoupled-DFIG fault ride-through strategy for enhanced stability performance during grid faults. *IEEE Trans. Sustain. Energy* **2010**, *1*, 152–162. [CrossRef]
12. Yang, L.; Xu, Z.; Ostergaard, J.; Dong, Z.Y.; Wong, K.P. Advanced control strategy of DFIG wind turbines for power system fault ride through. *IEEE Trans. Power Syst.* **2012**, *27*, 713–722. [CrossRef]
13. Kennedy, J.; Eberhart, R.C. Particle swarm optimisation. In Proceedings of the IEEE International Conference on Neural Networks, Perth, WA, Australia, 27 November–1 December 1995; pp. 1942–1948.
14. Storn, R.; Price, K. *Differential Evolution-A Simple and Efficient Adaptive Scheme for Global Optimization over Continuous Spaces*; Technical Report TR-95-012; International Computer Science Institute: Berkley, CA, USA, 1995.
15. Mohammadmehdi, S.; Rasoul, R.; Saad, M.; Amanullah, M.T.O.; Alex, S.; Tey, K.S.; Alireza, S.G. Simulation and hardware im-plementation of new maximum power point tracking technique for partially shaded PV system using hybrid depso method. *IEEE Trans. Sustain. Energy* **2015**, *6*, 850–862.
16. Huo, J.; Ma, L.; Yu, Y.; Wang, J. Hybrid algorithm based mobile robot localization using DE and PSO. In Proceedings of the 32nd Chinese Control Conference, Xi'an, China, 26–28 July 2013; pp. 5955–5959.
17. Wang, P.; Liang, L.; Ji, Y.; Liu, X.; Chen, S.; Xie, G.; Fan, L. Parameter identification of steam turbine governor system based on DEPSO algorithm. In Proceedings of the 2017 3rd IEEE International Conference on Control Science and Systems Engineering (ICCSSE); Institute of Electrical and Electronics Engineers (IEEE), Beijing, China, 17–19 August 2017; pp. 228–232.

18. Elgammal, A.A.A. Adaptive fuzzy sliding mode controller for grid interface ocean wave energy conversion. *J. Intell. Learn. Syst. Appl.* **2014**, *6*, 53–69. [CrossRef]
19. Hong, Y.; Waters, R.; Bostrom, C.; Eriksson, M.; Engstrom, J.; Leijon, M. Review on electrical control strategies for wave energy conversion systems. *Renew. Sustain. Energy Rev.* **2014**, *31*, 329–342. [CrossRef]
20. Lin, W.-M.; Hong, C.-M.; Huang, C.-H.; Ou, T.-C. Hybrid control of a wind induction generator based on grey-elman neural network. *IEEE Trans. Control. Syst. Technol.* **2013**, *21*, 2367–2373. [CrossRef]
21. Patra, J.C.; Pal, R.N. A functional link artificial neural network for adaptive channel equalization. *Signal Process.* **1995**, *43*, 181–195. [CrossRef]
22. Ou, T.-C.; Lu, K.-H.; Huang, C.-J. Improvement of transient stability in a hybrid power multi-system using a designed NIDC (novel intelligent damping controller). *Energies* **2017**, *10*, 488. [CrossRef]
23. Lin, W.; Lu, K.; Ou, T. Design of a novel intelligent damping controller for unified power flow controller in power system connected offshore power applications. *IET Gener. Transm. Distrib.* **2015**, *9*, 1708–1717. [CrossRef]
24. Vinal, P.; Vaibhav, G.; Shashank, H.; Nithin, V.G. Design of adaptive exponential functional link network-based nonlinear filters. *IEEE Trans. Circ. Syst. I. Regular Papers* **2016**, *63*, 1434–1442.
25. Brekken, T.K.A.; Ozkan-Haller, H.T.; Simmons, A. A methodology for large-scale ocean wave power time-series generation. *IEEE J. Ocean. Eng.* **2012**, *37*, 294–300. [CrossRef]
26. Cashman, D.P. Electrical Machine Characterisation and Analysis for Renewable Energy Applications. Ph.D. Thesis, University College Cork, Cork, Ireland, 2010.
27. Wang, L.; Chen, Z.-J. Stability analysis of a wave-energy conversion system containing a grid-connected induction generator driven by a wells turbine. *IEEE Trans. Energy Convers.* **2009**, *25*, 555–563. [CrossRef]
28. Kiran, D.R.; Palani, A.; Muthukumar, S.; Jayashankar, V. Steady grid power from wave energy. *IEEE Trans. Energy Convers.* **2007**, *22*, 539–540. [CrossRef]
29. Hogg, R.V.; McKean, J.W.; Craig, A.T. *Introduction to Mathematical Statistics*, 6th ed.; Prentice-Hall: New Jersey, NJ, USA, 2005.
30. Lin, W.M.; Hong, C.M. Intelligent approach to maximum power point tracking control strategy for variable-speed wind turbine generation system. *Energy* **2010**, *35*, 2440–2447. [CrossRef]
31. Lin, C.T.; Lee, G.C.S. *Neural Fuzzy Systems*; Prentice-Hall, Inc.: Upper Saddle River, NJ, USA, 1996.
32. Elsayed, S.M.; Sarker, R.A.; Essam, D.L. An improved self-adaptive differential evolution algorithm for optimization problems. *IEEE Trans. Ind. Inform.* **2012**, *9*, 89–99. [CrossRef]
33. Xin, B.; Chen, J.; Zhang, J.; Fang, H.; Peng, Z.-H. Hybridizing differential evolution and particle swarm optimization to design powerful optimizers: A review and taxonomy. *IEEE Trans. Syst. Man Cybern. Part C Appl. Rev.* **2011**, *42*, 744–767. [CrossRef]
34. Ben, N.; Li, L. A novel PSO-DE-based hybrid algorithm for global optimization. *Comp. Sci.* **2008**, *5227*, 156–163.
35. Wu, Y.C.; Lee, W.P.; Chien, C.W. Modified the performance of differential evolution algorithm with dual evolution strategy. *Int. Conf. Machine Learn. Comp.* **2011**, *3*, 57–63.
36. Yoo, S.J.; Choi, Y.H.; Park, J.B. Generalized predictive control based on self-recurrent wavelet neural network for stable path tracking of mobile robots: Adaptive learning rates approach. *IEEE Trans. Circuits Syst. I Regul. Pap.* **2006**, *53*, 1381–1394. [CrossRef]
37. Wai, R.J.; Li, C.M. Design of dynamic petri recurrent fuzzy neural network and its application to path-tracking control of nonho-lonomic mobile robot. *IEEE Trans. Indust. Electron.* **2009**, *56*, 2667–2683.
38. Lin, W.-M.; Hong, C.-M. A new Elman neural network-based control algorithm for adjustable-pitch variable-speed wind-energy conversion systems. *IEEE Trans. Power Electron.* **2010**, *26*, 473–481. [CrossRef]
39. Lu, K.-H.; Hong, C.-M.; Han, Z.; Yu, L. New Intelligent Control Strategy Hybrid Grey–RCMAC Algorithm for Ocean Wave Power Generation Systems. *Energies* **2020**, *13*, 241. [CrossRef]